05,07

Structural features and magnetic properties of non-stoichiometric $(1-x)BiFeO_3-xPbFeO_3$ solid solutions

© D.I. Rudsky[1], I.A. Verbenko[1], A.O. Galatova[1], S.P. Kubrin[1], A.V. Novikovsky[1], A.V. Nazarenko[2], Yu.V. Kabirov[3], A.R. Lebedinskaya[4], A.G. Rudskaya[3]

[1] Scientific Research Institute of Physics, Southern Federal University, Rostov-on-Don, Russia
[2] Federal State Budgetary Science Institute Federal Research Center Southern Research Center of RAS Southern Science Centre of the Russian Academy of Sciences (SSC RAS), Rostov-on-Don, Russia
[3] Faculty of Physics, Southern Federal University, Rostov-on-Don, Russia
[4] Southern Federal University, Academy of Architecture and Arts, Rostov-on-Don, Russia

E-mail: agrudskaya@sfedu.ru

Received August 7, 2025
Revised August 7, 2025
Accepted October 20, 2025

The article presents the results of studying the structures and magnetic properties of the compositions of the non-stoichiometric $(1-x)BiFeO_3-xPbFeO_3$ solid solution system with $x = 0.05$; 0.10; 0.15; 0.20; 0.25; 0.30; 0.50. It was found that at room temperature in the compositions $x = 0.05$ and 0.10 there is a rhombohedral phase $R3c$, in the compositions with $x = 0.15-0.30$ — a cubic phase $Pm\text{-}3m$ and in the composition with $x = 0.50$ — a rhombohedral phase $R\text{-}3c$. Using the γ-resonance method, it was found that Fe^{3+} ions are present in all compositions, which corresponds to non-stoichiometry in oxygen ions.

Keywords: $(1-x)BiFeO_3-xPbFeO_3$ solid-phase synthesis, X-ray diffraction, γ-resonance method, microstructure.

DOI: 10.61011/PSS.2025.10.62634.224-25

Introduction

It is a well-known fact that such physical properties as charge transfer, magnetic and ferroelectric properties in the oxygen-octahedral structures depend on the presence of d-elements in an octahedral oxygen environment. At the same time, the role of cations occupying cuboctahedral positions in the oxygen-octahedral structures is less well defined in their physical properties. Such cations, as a rule, are characterized by s-states (Ca, Sr, Ba). Cations with sp-states (Pb, Bi) define sp-hybridization of states in cation–oxygen systems.

In paper [1], the ferroelectric properties of lead-containing oxides with a perovskite structure are explained by the formation of asymmetric electronic configurations described by a combination of s- and p-atomic states characteristic of the Pb atom ($6s^26p^2$); similar potential is also reported for Bi atoms ($6s^26p^3$) and Tl atoms ($6s^26p$).

In Pb^{2+} and Bi^{3+} ions 6s-orbitals are more stable, than 6p-orbitals. The outer electron orbital $6s^2$ has a relatively large radial extent, which makes the ionic radius large, and this reduces the degree of overlap of 6p orbitals by the orbitals of the nearest neighboring anions. Such decline in overlapping leads to a compromised coupling $A-B$. The hybridization of 6s and 6p orbitals, which consists in the energetic splitting of these orbitals, leads to the polarization of the electrons of the outer orbitals, so that the effective ionic radius is significantly smaller on one side of the cations than on the other. This allows for the formation of a much stronger coupling on one side of the cation, and the energy generated by this coupling may be greater than the hybridization energy. It is for this reason that Pb^{2+} and Bi^{3+} ions are stabilized in most crystals with asymmetric anionic coordination.

The inert, unshared electron pair 6s in Bi^{3+} ions (in particular, in $BiFeO_3$) is the main cause of ferroelectricity. Such pairs are featuring high polarizability. The appearance of polarization can be visualized as a process of ordering such electron pairs in one direction. The presence in such structures of some magnetic ions [2,3], like Cr^{3+}, Mn^{2+}, Mn^{3+}, Mn^{4+}, Fe^{3+}, Fe^{2+}, Co^{3+}, Ni^{2+}, may additionally cause the formation of magnetic properties. In such cases, compounds and solid solutions are multiferroic.

The combination effects in a structure like perovskite ABO_3 of Bi^{3+} and Pb^{2+} ions in positions A and Fe^{3+}/Fe^{4+} ions in positions B may also be found in the solid solutions. $(1-x)BiFeO_3-xPbFeO_3$ [4,5]. Technically, the balance of valence states in FeO_3 requires either a four-valence state of Fe^{4+} ions [2,6,7], or the non-stoichiometry in the oxygen contents [8–11].

When the anion-deficient perovskites with crystallographic plane shifts in oxygen vacancies have been examined it demonstrated that in cases of lead-containing compounds (e.g., $Pb_2Fe_2O_5$), Pb ions may shift from the centers of the perovskite structure's cuboctahedral positions, thus, causing the ferroelectric spontaneous polarization that interacts with the ordering of the magnetic moments of transition cations such as Fe ions [12]. Such materials are potential multiferroics.

This paper provides the findings from the study of chemical composition, microstructures, structures, and magnetic properties of solid solutions. $(1-x)BiFeO_3-xPbFeO_3$ with $x = 0.05$, 0.10, 0.15, 0.20, 0.25, 0.30, 0.50.

1. Experiment

1.1. Solid-phase synthesis

The solid solutions $(1-x)BiFeO_3-xPbFeO_3$ with $0.05 \le x \le 0.30$ and spacing $\Delta x = 0.05$ and $x = 0.50$ were prepared by method of solid-state synthesis. Oxides Bi_2O_3, Fe_2O_3 and PbO with a chemical purity of 99.9 % were used as stock reagents. Before preparation of the studied samples, the reagents were additionally checked by X-ray diffraction analysis. The synthesis of samples of $(1-x)BiFeO_3-xPbFeO_3$system after stirring the stoichiometric mixtures in ethyl alcohol for one hour was carried out by annealing at temperatures of $T_1 = 700\,^\circ$C (3 h) and $T_2 = 750\,^\circ$C (3 h).

1.2. Microstructure

The microstructure of the samples of $(1-x)BiFeO_3-xPbFeO_3$ system was studied by method of scanning laser microscopy using KEYENCE VK-9700 scanning laser microscope (violet, 408 nm). The images are constructed using confocal microscopy. In this case, images that are in focus at different depths of the sample are sequentially captured. Everything above or below the focus is cut off by the confocal slit, leaving only the surface that is clear at this depth. Scanning takes place deep into the sample with a step of 0.2 μm, after which all the images obtained at different depths „are stitched", forming a clear two-dimensional picture. The samples were measured at a magnification of $\times$1000 and $\times$3000.

1.3. X-ray spectral analysis

Chemical composition of samples was checked using an X-ray fluorescent TXRF-spectrometer RFS-001 (Mo$K\alpha$-radiation) with Amptek detector having energy resolution of about 180 eV. X-ray fluorescence spectra were recorded and processed using UniverRS program. The composition of $PbFeO_3$ for the solid solutions $(1-x)BiFeO_3-xPbFeO_3$ was clarified based on the experimental data of X-ray fluorescence of Bi and Pb ions [13].

1.4. X-ray diffraction analysis

All samples were studied at room temperature by X-ray diffraction analysis using DRON-3M diffractometer (Cu$K\alpha$ radiation, Ni-filter) with Bragg-Brentano focusing ($\theta-2\theta$). The diffraction profiles were registered within the range of angles $20^\circ \le 2\theta \le 60^\circ$ in the step-by-step scanning of the sample-detector with a step of 0.02° and the pulse set time $\tau = 2$ s at each point. This range of angles 2θ was selected because it includes the most intense diffraction peaks. The extension of this range toward $2\theta \ge 60^\circ$ gives the possibility for the refinement taking into consideration the weak peaks of higher orders of reflections. At the same time a strong overlapping of these peaks is observed, which, of course, does not improve the results of the structural parameters refinement. The refinement of the structural parameters was carried out using a computer program PowderCell 2.4.

1.5. Mössbauer spectroscopy

Mössbauer spectra are measured using MS1104Em spectrometer. ^{57}Co in the matrix of Cr was used as a source of γ-quanta. The model was interpreted in SpecrRelax [14]. Isomer shifts are given relative to α-Fe.

2. Results and discussion

The chemical composition of the samples annealed at $T_1 = 700$ and $T_2 = 750\,^\circ$C showed (Figure 1) that they are characterized by the ratio of the content of Bi and Pb ions, which was incorporated in the initial mixtures of oxides. Figure 2 shows the photos of microstructures of samples of $(1-x)BiFeO_3-xPbFeO_3$ after synthesis at $T_1 = 700\,^\circ$C ($x = 0.50$) and after synthesis at $T_2 = 750\,^\circ$C ($x = 0.05$, 0.10, 0.15, 0.20, 0.25, 0.30, 0.50). The microstructure of samples on cleavage represents itself the mixture of „nanoscale" crystallites (0.5–1 μm). In some samples there are large crystallites with a size of 4–5 μm. In compositions with $x = 0.05, 0.30$ and 0.50, a fairly noticeable increase in the number of „large" crystallites is observed with higher annealing temperature. For other compositions with $x = 0.10$ and 0.20, an increase in the annealing temperature does not lead to noticeable changes in the crystallite sizes.

Fragments of X-ray diffraction patterns of compositions of $(1-x)BiFeO_3-xPbFeO_3$ system after synthesis at $T_2 = 750\,^\circ$C are shown in Figure 3. The diffraction patterns show all Bragg peaks characteristic of the perovskite type structures. In addition to the peaks corresponding to the main phases $(1-x)BiFeO_3-xPbFeO_3$, there are also peaks of impurity phases on the diffraction patterns. Table 1 shows concentrations of the perovskite (C_1) and impurity phases $Bi_2Fe_4O_9$ (C_2), $Bi_{25}FeO_{40}$ (C_3) and Pb_2BiO_4 (C_4).

It's worth mentioning that after repeated synthesis at $T_2 = 750\,^\circ$C in compositions with $x = 0.05-0.20$ the impurity phases of $Bi_{25}FeO_{40}$ and $Bi_2Fe_4O_9$ are observed in the amount from 2.4 ($x = 0.15$) to 25 % ($x = 0.05, 0.10$ and 0.20). Composition with $x = 0.50$ is characterized

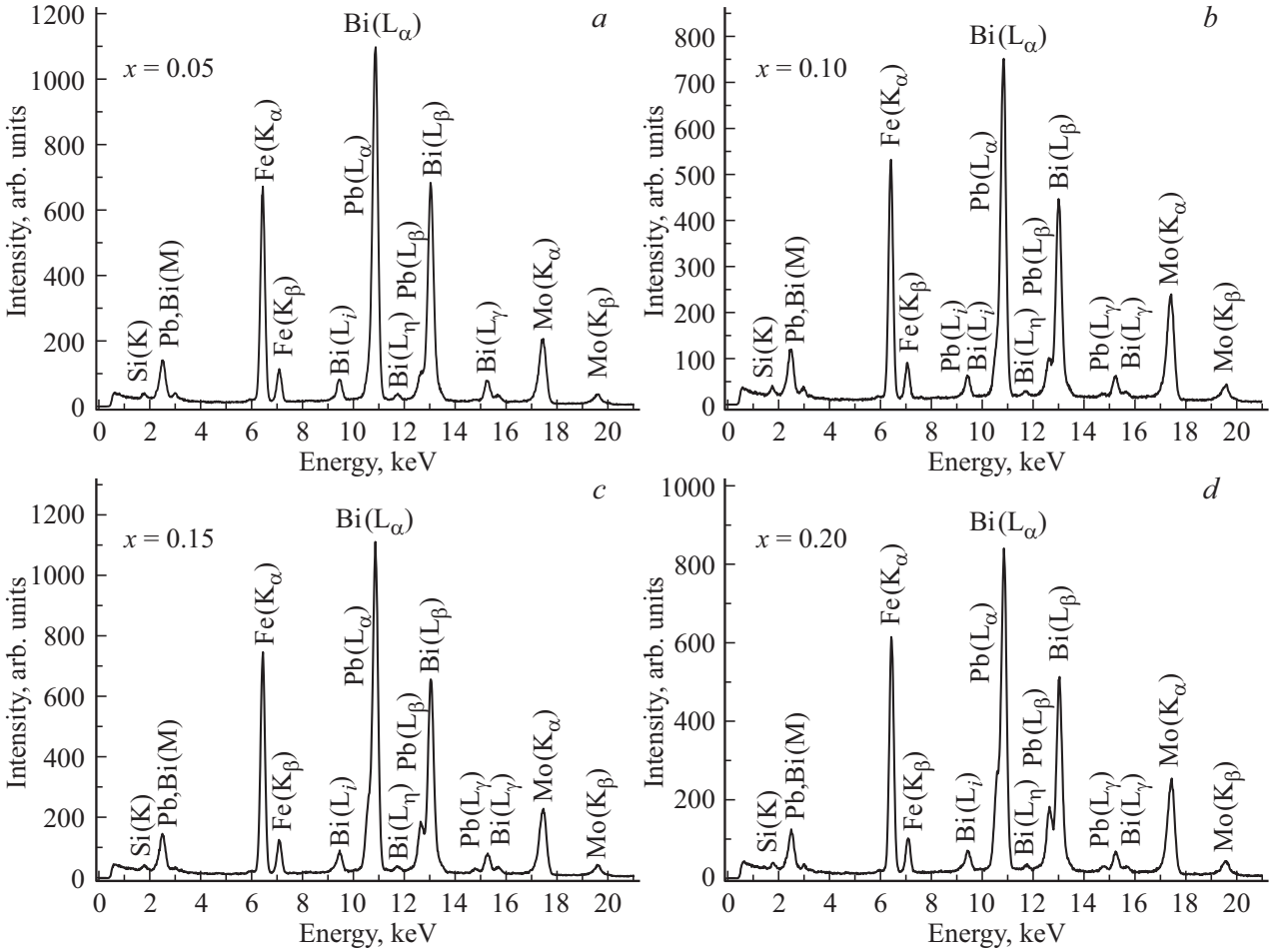

Figure 1. X-ray fluorescent spectra of the compositions of system $(1-x)BiFeO_3-xPbFeO_3$, prepared at $T_2 = 750\,^{\circ}C$: *a*) $x = 0.05$; *b*) $x = 0.10$; *c*) $x = 0.15$; *d*) $x = 0.20$; *e*) $x = 0.25$; *f*) $x = 0.30$; *g*) $x = 0.50$.

Table 1. Phase composition of samples in $(1-x)BiFeO_3-xPbFeO_3$ system at a room temperature after sequential synthesis at $T_1 = 700$ and $T_2 = 750\,^{\circ}C$

T, °C	x	$(1-x)$BFO$-x$PFO C_1, %	$Bi_2Fe_4O_9$ C_2, %	$Bi_{25}FeO_{40}$ C_3, %	Pb_2BiO_4 C_4, %
700	0.05	60.0	27.2	12.8	–
	0.10	55.2	30.9	13.9	–
	0.15	76.1	17.3	6.6	–
	0.20	84.8	12.8	2.5	–
	0.25	100.0	–	–	–
	0.30	100.0	–	–	–
	0.50	43.6	–	–	56.4
750	0.05	94.2	1.8	4.0	–
	0.10	75.8	17.6	6.6	–
	0.15	97.6	–	2.4	–
	0.20	74.9	20.1	5.0	–
	0.25	100.0	–	–	–
	0.30	100.0	–	–	–
	0.50	45.0	5.2	–	49.8

Note. C_i $(i = 1, \ldots, 4)$ — concentrations of phases defined with an accuracy of $\pm 0.5\,\%$.

by the mixture of phases $Bi_2Fe_4O_9$ ($C = 5.2\,\%$), Pb_2FeO_4 ($C = 49.8\,\%$) and and perovskite rhombohedral $R3c$ phase $Bi_{0.5}Pb_{0.5}FeO_{3-\delta}$ ($C = 45\,\%$).

Table 2 shows the structural parameters of the compounds of $(1-x)BiFeO_3-xPbFeO_3$ system with $x = 0.10$, 0.15 and 0.50 after their synthesis at $T_2 = 750\,^{\circ}C$ and results of refinement of atomic parameters for these compounds: parameters of the lattice cells (a_H, c_H and a_p), positional (x, y, z) and isotropic parameters of Debye-Waller factor (B), structures reliability parameter (R_p), as well as parameters corresponding to the parameters of rhombohedral (a_R, α_R) perovskite sub-lattices calculated by formulae from [15].

In the spatial group $R3c$ (No. 161) A type atoms are in the fixed positions A(Bi/Pb) — 6*a* (0; 0; 1). For atoms of B type the coordinate z is a free (refined) parameter: B(Fe) — 6*a* $(0; 0; z)$, and oxygen atoms have in the cell the position of 18*e* $(x; 0; 1/4)$. Positions of atoms for the spatial group $R\text{-}3c$ (No. 167) are as follows: A(Bi/Pb) — 6*a* $(0; 0; 1/4)$, B(Fe) — 6*b* (0; 0; 0), O — 18*e* $(x; 0; 1/4)$. Positions of atoms for the spatial group $Pm\text{-}3m$ (No. 221) are as follows:

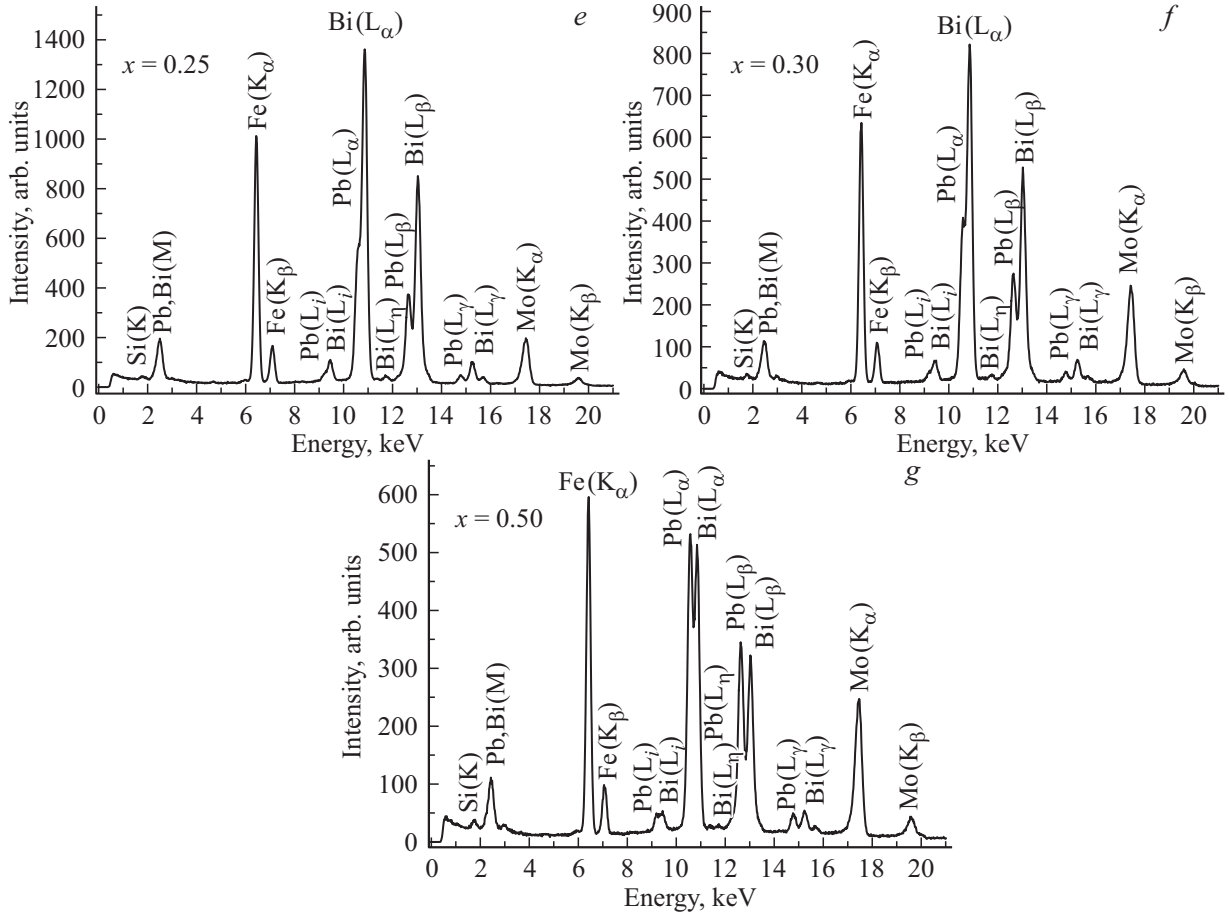

Figure 1 (*Continued*).

A(Bi/Pb) — 1a (0; 0; 0), B(Fe) — 1b (0.5; 0.5; 0.5), O — 3c (0; 0.5; 0.5).

Figure 4 shows the dependences of the volumes of lattice cells V_{ABO3} per one formula unit ABO_3 and the area of existence at room temperature of rhombohedral phases $R3c$ and R-3c and cubic phases Pm-3m. The box window in Figure 4 shows the relations of the parameters c_H/a_H, where a_H and c_H are the parameters of the lattice cells of the perovskite structure in hexagonal systems. Parameters $\mathbf{a}_H = \mathbf{a}_p + \mathbf{b}_p$ and $\mathbf{c}_H = 2(\mathbf{a}_p + \mathbf{b}_p + \mathbf{c}_p)$, where $\mathbf{a}_p$, $\mathbf{b}_p$ and $\mathbf{c}_p$ — translations of the perovskite structure. It can be seen that after synthesis at $T_2 = 750\,^\circ$C, compositions with $x = 0.05$ and 0.10 are characterized by a rhombohedral phase $R3c$ and a decrease in c_H/a_H with higher x due to a decrease in the period c_H, which corresponds to a decline in spontaneous polarization. Note that the region of existence of $R3c$ phase narrows after synthesis at $T_2 = 750\,^\circ$C compared to the region of this phase after initial synthesis at $T_1 = 700\,^\circ$C. Compounds with $x = 0.15{-}0.30$ are characterized by cubic phases Pm-3m. Compound with $x = 0.50$ is characterized by the rhombohedral phase R-3c with the ratio of c_H/a_H, equal 2.46. Noteworthy is the difference between R-3c phase and $R3c$ phase, which is explained by the fact that in this phase the perovskite rhombohedral cell is compressed along the third-order axis, in contrast to the stretching of the cell along the third-order polar axis in $R3c$ phase, which is due to the presence of ferroelectric spontaneous polarization.

The Mössbauer spectra of ceramic samples of solid solutions $(1-x)BiFeO_3{-}xPbFeO_3$synthesized at temperatures $T_1 = 700$ and $T_2 = 750\,^\circ$C are shown in Figure 5. The parameters of the components of these spectra are shown as concentration dependence graphs in Figures 6–8. Two paramagnetic doublets are observed on the spectra of samples with $x \leq 0.20$, with their parameters close to those observed for $Bi_2Fe_4O_9$ [16], which is a characteristic impurity for $BiFeO_3$ solid solutions[17,18]. Figure 9 shows the concentration dependence of the total area of the doublet components corresponding to the impurity $Bi_2Fe_4O_9$. It can be seen that the area of these components, and, consequently, the concentration of the impurity phase $Bi_2Fe_4O_9$, decreases linearly with the growth of x. At the same time, for samples with $T_2 = 750\,^\circ$C, the impurity concentration is about 2.5 times lower than for samples with $T_1 = 700\,^\circ$C.

The spectrum of the sample with $x \leq 0.05$ obtained at $T_1 = 700\,^\circ$C contains two Zeeman sextets, apart from the impurity phase doublets. Isomeric shifts of the sextets

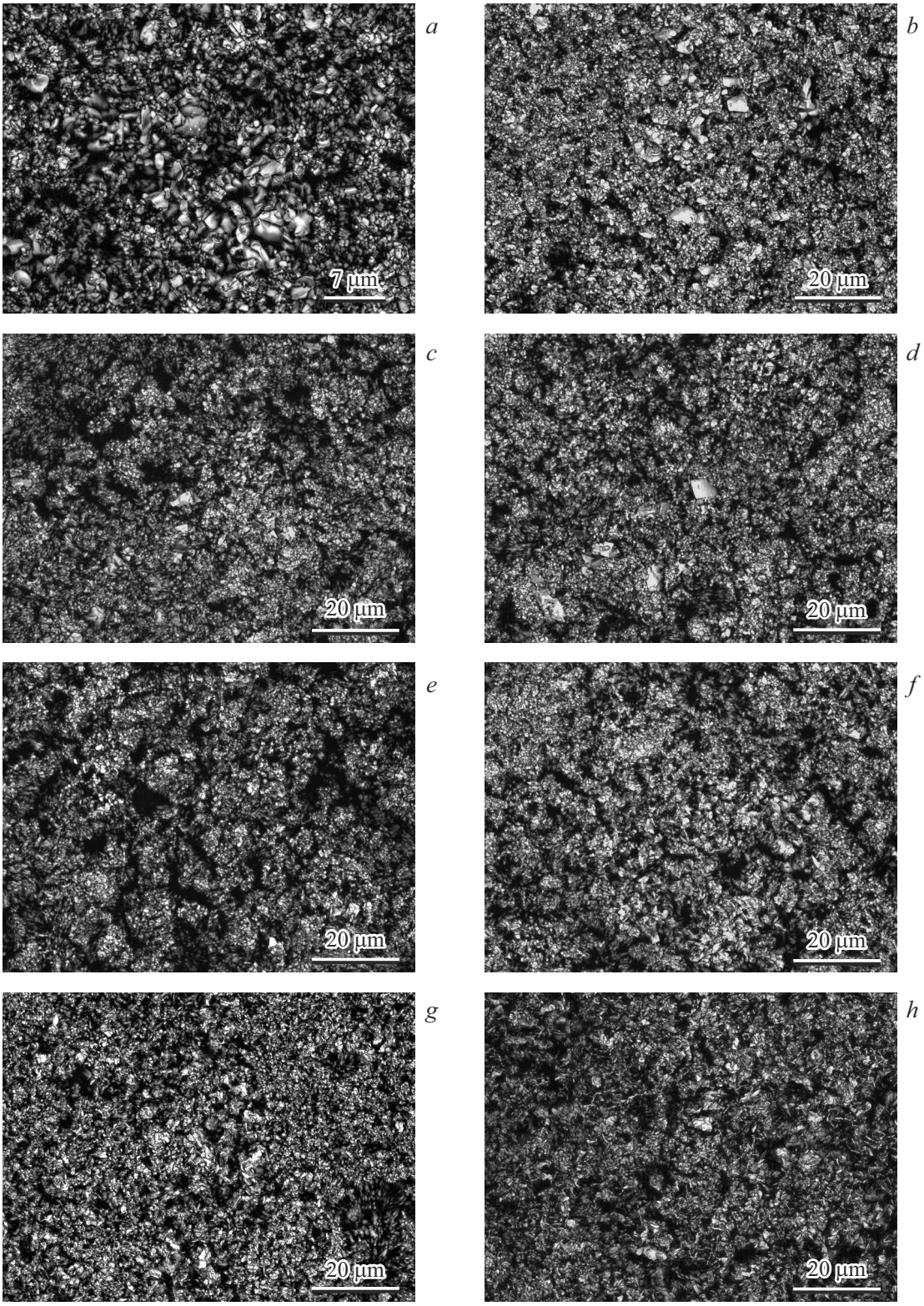

Figure 2. Microstructures of $(1-x)BiFeO_3-xPbFeO_3$ system compounds after synthesis at $T_1 = 700\,^\circ C$ ($x = 0.50$) and after synthesis at $T_2 = 750\,^\circ C$ with $x = 0.05$, 0.10, 0.15, 0.20, 0.25, 0.30, 0.50. *a*) $x = 0.05$ ($T_2 = 750\,^\circ C$), *b*) $x = 0.10$ ($T_2 = 750\,^\circ C$), *c*) $x = 0.15$ ($T_2 = 750\,^\circ C$), *d*) $x = 0.20$ ($T_2 = 750\,^\circ C$), *e*) $x = 0.25$ ($T_2 = 750\,^\circ C$), *f*) $x = 0.30$ ($T_2 = 750\,^\circ C$), *g*) $x = 0.50$ ($T_1 = 700\,^\circ C$), *h*) $x = 0.50$ ($T_2 = 750\,^\circ C$).

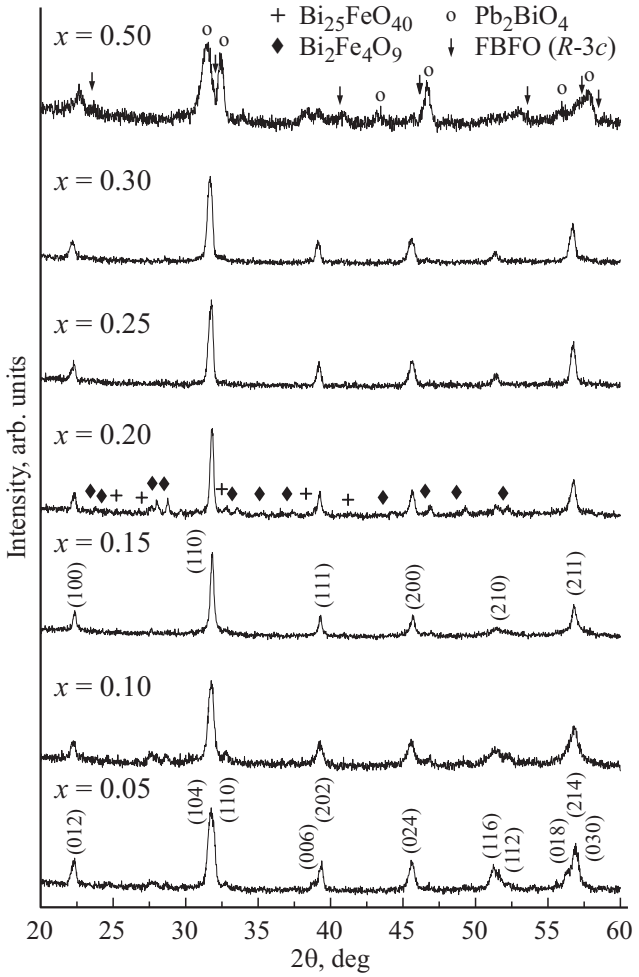

Figure 3. X-ray diffraction patterns at a room temperature for the compounds of $(1-x)BiFeO_3-xPbFeO_3$ with $x = 0.05$, 0.10, 0.15, 0.20, 0.25, 0.30, 0.50 after synthesis at $T_2 = 750\,^{\circ}C$. Miller indices are given for the rhombohedral phase $R3c$ ($x = 0.05$) and cubic phase $Pn\text{-}3m$ ($x = 0.20$). Symbols (+), (♦) and (°) denote the X-ray diffraction reflections of the impurity phases $Bi_{25}FeO_{40}$, $Bi_2Fe_4O_9$ and Pb_2BiO_4 respectively; symbol (↓) denotes the perovskite rhombohedral $R\text{-}3c$ phase ($x = 0.50$).

(0.39 mm/s) correspond to Fe^{3+} ions in the octahedral environment of [19], characteristic of compounds with the perovskite structure [20]. The sextet S1 has a lower effective magnetic field strength than S2. Additionally, the ratio of the quadrupole shifts ε_{S2} to ε_{S1} is approximately 2, which indicates the presence of a spatial spin-modulated structure (SSMS), as in $BiFeO_3$ [21,22]. That is, the sextet with a lower field value corresponds to Fe^{3+} ions, where magnetic moments are oriented perpendicular to the axis of symmetry of the third order, and the sextet with a higher field value corresponds to Fe^{3+} ions with the orientation of the moments along this axis. When $x \geq 0.1$, another S3 sextet with an isomeric shift $\sim 0.31-0.35$ mm/s and lower intensities of the effective magnetic fields compared to S1 and S2 is observed on Mössbauer spectra. The isomeric shift of S3 sextet corresponds to Fe^{3+} ions with a coordination number of 5. Thus, the S3 sextet is associated with the formation of oxygen vacancies as a result of the charge compensation when Bi^{3+} ions are replaced by Pb^{2+} ions, as for other systems based on $BiFeO_3$ with heterovalent substitution [23,24]. At the same time, already at $x = 0.1$, the SSMS is destroyed and the spectra have the form of a homogeneous spin structure, as can be seen by changing the parameters S1 and S2. Thus, for $x \geq 0.1$ of $(1-x)BiFeO_3-xPbFeO_3$ system with $T_1 = 700\,^{\circ}C$ the sextets S1 and S2 correspond to Fe^{3+} ions in the octahedral oxygen environment. The value of isomer shift and magnetic field of S2 sextet is leas than for S1, and with the growth of x the values of these parameters for S1 decline (Figure 6, *a* and 8, *a*). Apparently, S1 sextet corresponds to Fe^{3+} ions in octahedra that directly border the oxygen polyhedra corresponding to S3 sextet. Higher absolute values of the quadrupole shifts of all sextets, as well as a broadening of their lines, indicate an increase in the degree of symmetrical distortions of the nearest environment of Fe^{3+} ions and growth of crystallographic inhomogeneities.

Similar situation is observed for the spectra of solid solutions $(1-x)BiFeO_3-xPbFeO_3$, obtained at $T_2 = 750\,^{\circ}C$. However, for the spectra with $x = 0.1$ the SSMS still can be observed, with its further destruction at $x = 0.15$. The sextet corresponding to Fe^{3+} ions with a coordination number of 5 also appears at a higher value of $x = 0.15$. Otherwise, the behavior of Mössbauer spectra parameters is repeated with an increase of x (Figures 6, *b* and 8, *b*).

Hyperfine magnetic fields on ^{57}Fe nuclei of all three Zeeman sextets vary slightly in the concentration range $0.10 \leq x \leq 0.25$ for both systems with $T_1 = 700$ and

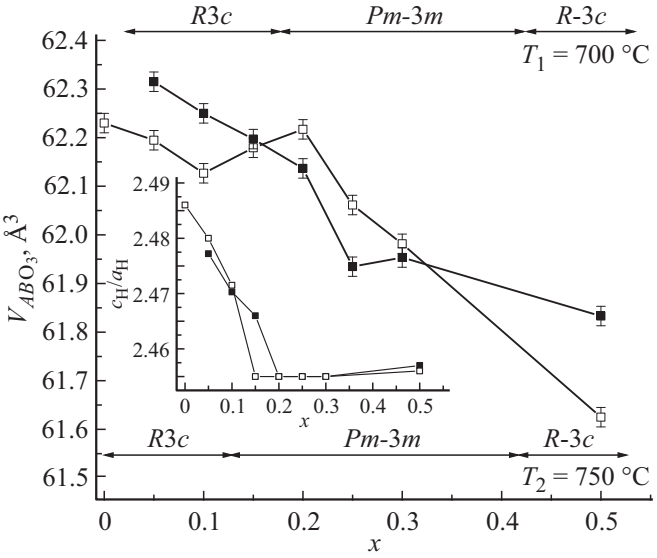

Figure 4. Dependences of the volumes of lattice cells per one formula unit ABO_3 and the area of existence at room temperature of rhombohedral phases $R3c$ and $R\text{-}3c$ and cubic phase $Pm\text{-}3m$ for solid solutions $(1-x)BiFeO_3-xPbFeO_3$. The insert window shows the ratio of parameters. c_H/a_H (■ — $T_1 = 700\,^{\circ}C$; □ — $T_2 = 750\,^{\circ}C$).

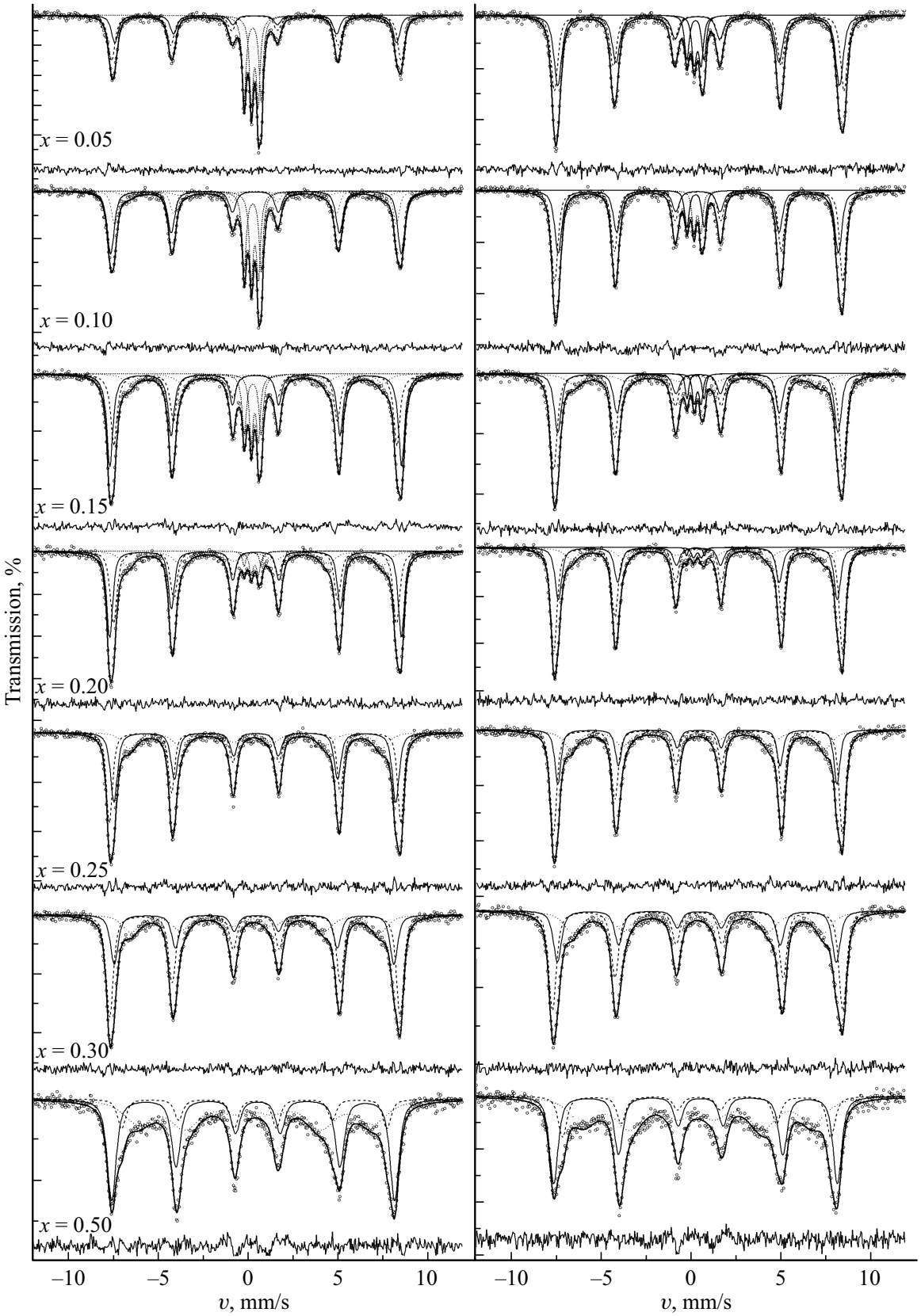

Figure 5. Mössbauer spectra of samples of solid solutions $(1-x)BiFeO_3-xPbFeO_3$ synthesized at *a*) $T_1 = 700\,^{\circ}C$ and *b*) $T_2 = 750\,^{\circ}C$, measured at room temperature.

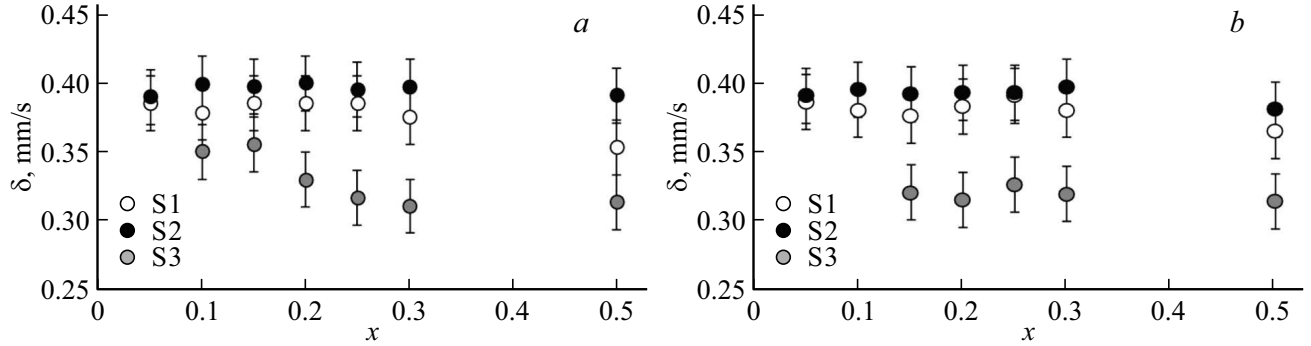

Figure 6. Concentration dependences of the isomeric shifts of the components of Mossbauer spectra of samples of solid solutions $(1-x)BiFeO_3-xPbFeO_3$ synthesized at *a*) $T_1 = 700\,^\circ C$ and *b*) $T_2 = 750\,^\circ C$.

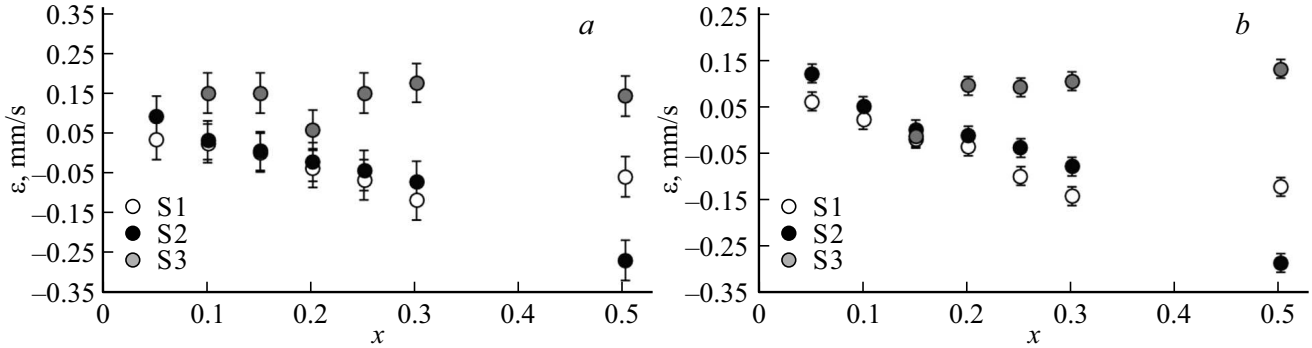

Figure 7. Concentration dependences of the magnitude of quadrupole shifts of the components of Mossbauer spectra of solid solutions samples $(1-x)BiFeO_3-xPbFeO_3$ synthesized at *a*) $T_1 = 700\,^\circ C$ and *b*) $T_2 = 750\,^\circ C$.

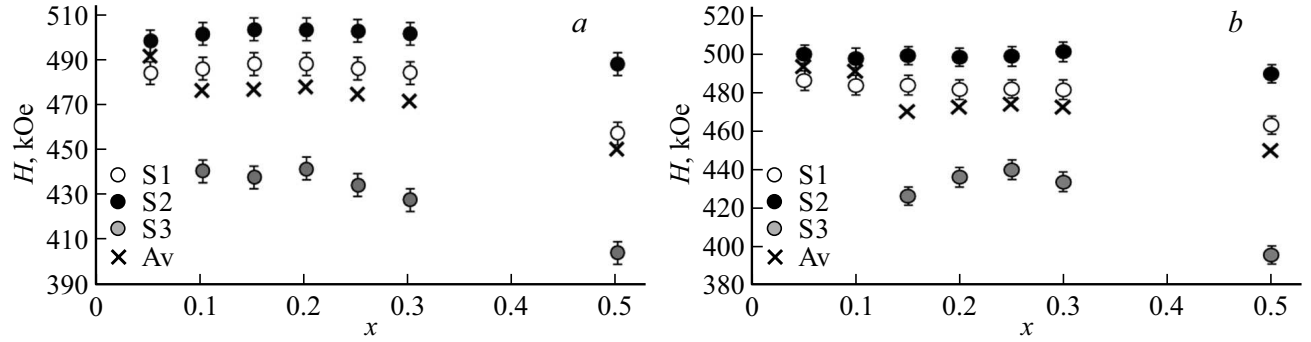

Figure 8. Concentration dependencies of the effective magnetic fields intensity on ^{57}Fe nuclei of the components of Mössbauer spectra of solid solutions samples $(1-x)BiFeO_3-xPbFeO_3$, synthesized at *a*) $T_1 = 700\,^\circ C$ and *b*) $T_2 = 750\,^\circ C$.

$T_2 = 750\,^\circ C$. At $x \geq 0.3$, the magnetic field strengths begin to decrease. The average values of hyperfine fields decrease, which means that the values of the magnetic moments of Fe^{3+} ions should go down. Hyperfine effective magnetic field on ^{57}Fe nuclei is related to the magnetic moment of Fe^{3+} ion (μ_{Fe}) by the following expression [25]: $H_{eff} = -\alpha \cdot \mu_{Fe}$, where α — hyperfine bond constant. In study [21] the magnitude of $\alpha = -133.5\,kOe$ was evaluated. Using this value α and taking the average values of the hyperfine magnetic fields of S1–S3 as H_{eff}, the μ_{Fe} was evaluated and its concentration dependence was plotted (Figure 10). The dependence patterns of the samples with $T_1 = 700$ and $T_2 = 750\,^\circ C$ are approximately the same. In both cases, the values of μ_{Fe} decline to $\approx 3.55\mu_B$, which remains unchanged in the range of $0.15 \leq x \leq 0.25$, and continues to decline with further growth of x. At the same time, the system with $T_1 = 700\,^\circ C$ reaches the value of $\mu_{Fe} \approx 3.55\mu_B$ faster, due to the earlier manifestation of oxygen deficiency. The plateau in $0.15 \leq x \leq 0.25$ region is apparently due to partial compensation of μ_{Fe} caused by structural changes.

Table 2. Structural parameters $(1-x)BiFeO_3-xPbFeO_3$ at room temperature for the compounds with $x = 0.10, 0.15$ and 0.50 synthesized at $T_2 = 750\,^\circ C$

x	0.10	0.15	0.50
Spatial group	$R3c$	$Pm\text{-}3m$	$R\text{-}3c$
a_H, c_H, Å	5.587(3); 13.807(4)	–	5.506(3); 13.438(4)
a_p, Å	–	3.963(3)	–
a_R, Å	3.962(3)	–	3.889(3)
α_R, deg	89.66(2)	90.00	90.14(2)
V_{ABO3}, Å^3	62.20(2)	62.22(2)	58.81(2)
c_H/a_H	2.47(1)	2.46(1)	2.46(1)
C_p, %	75.8(4)	97.6(5)	45.0(2)
Bi/Pb — $x;y;z$	0; 0; 1	0; 0; 0	0; 0; 0.25
B(Bi/Pb), Å^2	0.1	0.15	0.15
Fe — $x;y;z$	0; 0; 0.25	0.5; 0.5; 0.5	0; 0; 0
B(Fe), Å^2	0.1	0.15	0.15
O — $x;y;z$	0.475; 0.015; 0.955	0; 0.5; 0.5	0.446; 0; 0.25
B(O), Å^2	0.1	0.05	0.1
R_p, %	5.4	5.7	6.7
R_{wp}, %	6.8	7.3	8.4
R_{exp}, %	0.4	0.5	0.2
$l_{Bi/Pb-O}$, Å	2.287(3)	2.807(3)	2.458(3)
$l_{Bi/Pb-O}$, Å	2.686(3)	–	3.049(3)
$l_{Bi/Pb-O}$, Å	3.040(3)	–	2.762(3)
l_{Fe-O}, Å	1.776(2)	1.985(2)	1.967(2)
l_{Fe-O}, Å	2.355(2)	–	–
l_{O-O}, Å	2.686(3)	2.807(3)	2.801(3)
l_{O-O}, Å	2.827(3)	–	2.762(3)
l_{O-O}, Å	2.811(3)	–	2.801(3)
l_{O-O}, Å	2.936(3)	–	–

Note. l_{A-O}, l_{B-O}, l_{O-O} — lengths of the interatomic bonds.

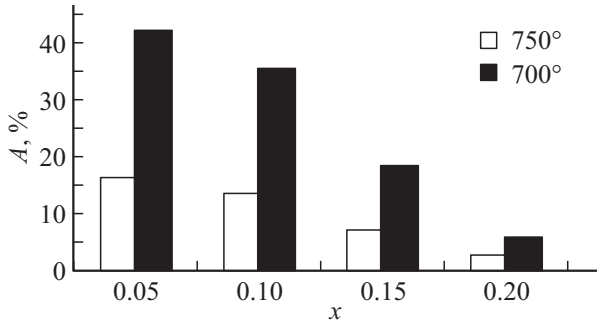

Figure 9. Concentration dependences of the total area of doublet components of the corresponding $Bi_2Fe_4O_9$ impurity in samples of solid solutions $(1-x)BiFeO_3-xPbFeO_3$, synthesized at $T_1 = 700\,^\circ C$ (black columns) and $T_2 = 750\,^\circ C$ (white columns).

3. Conclusion

The major peculiarity of the structures of $(1-x)BiFeO_3-xPbFeO_3$ system is that between $R3c$ ($x = 0, 0.05$ and 0.10) and $R\text{-}3c$ ($x = 0.50$) phases at room temperature the cubic phase $Pm\text{-}3m$ ($x = 0.15, 0.20, 0.25, 0.30$) is observed. The presence of cubic phase at room temperature indicates that phase transitions in the corresponding compounds occur at lower temperatures.

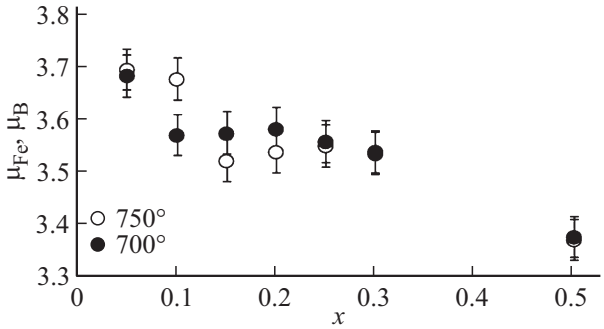

Figure 10. Concentration dependences of magnetic moments of Fe^{3+} ions in the samples of solid solutions $(1-x)BiFeO_3-xPbFeO_3$, synthesized at $T_1 = 700\,^\circ C$ (black circles) and $T_2 = 750\,^\circ C$ (white circles).

Thus, the Mossbauer study of the solid solutions compounds of $(1-x)BiFeO_3-xPbFeO_3$ system with $T_1 = 700$ and $T_2 = 750\,^\circ C$ showed that all iron ions in the studied solid solutions are in Fe^{3+} state. In compounds with $x = 0.10$ ($T_1 = 700\,^\circ C$) and $x = 0.15$ ($T_2 = 750\,^\circ C$), the spatial spin-modulated structure is destroyed. A rise in the ion concentration Pb^{2+} leads to the appearance of oxygen vacancies at Fe^{3+}, rather than to the formation of a mixed valence state of $Fe^{3+} \leftrightarrow Fe^{4+}$. Oxygen deficiency leads to a decrease in μ_{Fe}, which weakens the magnetic properties of this system.

Funding

The study was supported by the Ministry of Science and Higher Education of the Russian Federation (State assignment in the field of research. project No. FENW-2023-0010/GZ0110/23-11-IF).

Conflict of interest

The authors declare that they have no conflict of interest.

References

[1] J.B. Goodenough, J.M. Longo. Group III, v. 4a. / Ed. K.-H. Hellwege. Springer-Verlag, Berlin–Heidelberg–N.Y. (1970). P. 207–262.
[2] J.B. Goodenough, J. Zhou. Sci. Technol. Adv. Mater. **16**, *3*, 036003 (2015).
[3] R. Asih, M. Gufron, Darminto. AIP Conf. Proceed. **1554**, *1*, 50 (2013). http://dx.doi.org/10.1063/1.4820281
[4] I.O. Troyanchuk, O.S. Mantytskaya, A.N. Chobot, N.V. Tereshko. Phys. Solid State **51**, *10*, 2105 (2009).
[5] I.O. Troyanchuk, M.V. Bushinsky, D.V. Karpinsky, V. Sirenko, V. Sikolenko, V. Efimov. Eur. Phys. J. B **73**, *3*, 375 (2010).

[6] T. Tsuchiya, H. Saito, M. Yoshida, T. Katsumata, T. Ohba, Y. Inaguma, T. Tsurui, M. Shikano. MRS Online Proceed. Library **988**, 9880916 (2006). https://doi.org/10.1557/PROC-988-0988-QQ09-16
[7] A. Erkişi, E.K. Yíldírím, G. Gökoğlu. Int. J. Mod. Phys. B **28**, *29*, 1450205 (2014).
[8] J. Hadermann, A.M. Abakumov, I.V. Nikolaev, E.V. Antipov, G. Van Tendeloo. Solid State Sci. **10**, *4*, 382 (2008).
[9] M. Wang, G. Tan. Mater. Res. Bull. **46**, *3*, 438 (2011).
[10] A.M. Abakumov, J. Hadermann, S. Bals, I.V. Nikolaev, E.V. Antipov, G. Van Tendeloo. Angew. Chemie Int. Ed. **45**, *40*, 6697 (2006).
[11] I.V. Nikolaev, H. D'Hondt, A.M. Abakumov, J. Hadermann, A.M. Balagurov, I.A. Bobrikov, D.V. Sheptyakov, V.Yu. Pomjakushin, K.V. Pokholok, D.S. Filimonov, G. Van Tendeloo, E.V. Antipov. Phys. Rev. B **78**, *2*, 024426 (2008).
[12] A.M. Abakumov, J. Hadermann, G. Van Tendeloo, E.V. Antipov. J. Am. Ceram. Soc. **91**, *6*, 1807 (2008).
[13] A.S. Golofastova, N.M. Novikovsky, V.M. Raznomazov, A.V. Pavlenko, I.A. Verbeno, D.A. Sarychev, L.A. Reznichenko, A.V. Makhiboroda. UPF **4**, *1*, 32 (2016). (in Russian).
[14] M.E. Matsnev, V.S. Rusakov. AIP Conf. Proc. **1489**, *1*, 178 (2012).
[15] K.A. Googlev, A.T. Kozakov, A.G. Kochur, A.V. Nikolskii, A.G. Rudskaya, S.I. Shevtsova. Physica Scripta **99**, *6*, 0659a6 (2024).
[16] G.C. Papaefthymiou, A.J. Viescas, J.-M. Le Breton, H. Chiron, J. Juraszek, T.-J. Park, S.S. Wong. Current Appl. Phys. **15**, *3*, 417 (2015).
[17] V.M. Denisov, N.V. Volkov, L.A. Irtyugo, G.S. Patrin, L.T. Denisova. Phys. Solid State **54**, *6*, 1312 (2012).
[18] I.A. Verbenko, Yu.M. Gufan, S.P. Kubrin, A.A. Amirov, A.A. Pavelko, V.A. Aleshin, L.A. Shilkina, O.N. Razumovskaya, L.A. Reznichenko, I.A. Osipenko, D.A. Sarychev, A.B. Batdalov. Bull. RAS: Phys. **74**, *8*, 1141 (2010).
[19] F. Menil. J. Phys. Chem. Solids **46**, *7*, 763 (1985).
[20] I.P. Raevski, S.P. Kubrin, S.I. Raevskaya, D.A. Sarychev, S.A. Prosandeev, M.A. Malitskaya. Phys. Rev. B **85**, *22*, 224412 (2012).
[21] V.S. Pokatilov, V.V. Pokatilov, A.S. Sigov. Phys. Solid State **51**, *3*, 552 (2009).
[22] V.S. Rusakov, V.S. Pokatilov, A.S. Sigov, M.E. Matsnev, T.V. Gubaidulina. JETP Lett. **100**, *7*, 463 (2014).
[23] A.T. Kozakov, A.G. Kochur, V.I. Torgashev, A.A. Bush, V.Ya. Shkuratov, S.P. Kubrin, A.V. Nikolskii, K.A. Googlev. J. Electron Spectrosc. & Related Phenomena **189**, 106 (2013).
[24] A.T. Kozakov, A.G. Kochur, V.I. Torgashev, K.A. Googlev, S.P. Kubrin, V.G. Trotsenko, A.A. Bush, A.V. Nikolskii. J. Alloys. Compd. **664**, 392 (2016).
[25] M.B. Stearns. Phys. Rev. B **4**, *11*, 4081 (1971).

Translated by T.Zorina